


# Construction of zinc–organic frameworks by flexible aliphatic dicarboxylates plus 2-(1H-imidazolyl-1-methyl)-1H-benzimidazole ligand

Qiuying Huang, Xiuxiu Wang, Ting Li & Xiangru Meng


To cite this article: Qiuying Huang, Xiuxiu Wang, Ting Li & Xiangru Meng (2015) Construction of zinc–organic frameworks by flexible aliphatic dicarboxylates plus 2-(1H-imidazolyl-1-methyl)-1H-benzimidazole ligand, *Journal of Coordination Chemistry*, 68:1, 88-105, DOI: [10.1080/00958972.2014.984702](https://doi.org/10.1080/00958972.2014.984702)



To link to this article: <http://dx.doi.org/10.1080/00958972.2014.984702>

 View supplementary material 


 Accepted author version posted online: 06 Nov 2014.  
Published online: 02 Dec 2014.

 Submit your article to this journal 

 Article views: 74

 View related articles 

 View Crossmark data 

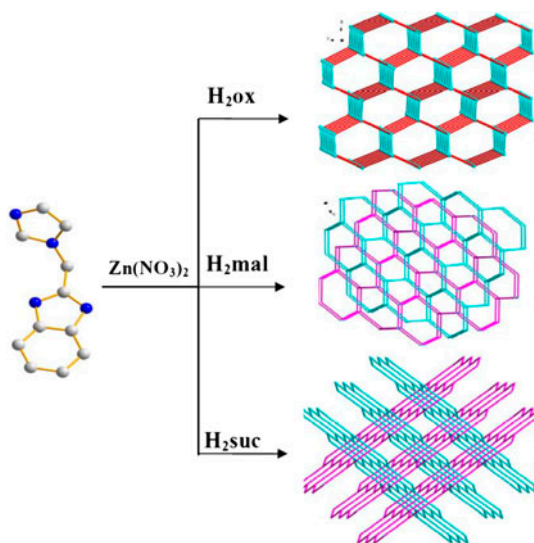
 Citing articles: 2 View citing articles 

## Construction of zinc–organic frameworks by flexible aliphatic dicarboxylates plus 2-(1*H*-imidazolyl-1-methyl)-1*H*-benzimidazole ligand

QIUYING HUANG<sup>†‡</sup>, XIUXIU WANG<sup>‡</sup>, TING LI<sup>‡</sup> and XIANGRU MENG<sup>\*‡</sup>

<sup>†</sup>Department of Chemical Engineering, Henan Polytechnic Institute, Nanyang, PR China  
<sup>‡</sup>The College of Chemistry and Molecular Engineering, Zhengzhou University, Zhengzhou, PR China

(Received 24 July 2013; accepted 16 August 2014)



Three new Zn(II) complexes, [Zn(ox)(imb)] (**1**), [Zn<sub>2</sub>(mal)<sub>2</sub>(imb)<sub>2</sub>] (**2**) and [Zn(suc)(imb)]·H<sub>2</sub>O (**3**), have been synthesized and structurally characterized. IR spectra, PXRD patterns, thermogravimetric curves, and photoluminescence spectra are addressed.

Three new Zn(II) complexes, [Zn(ox)(imb)] (**1**), [Zn<sub>2</sub>(mal)<sub>2</sub>(imb)<sub>2</sub>] (**2**), and [Zn(suc)(imb)]·H<sub>2</sub>O (**3**) (imb = 2-(1*H*-imidazolyl-1-methyl)-1*H*-benzimidazole, H<sub>2</sub>ox = oxalic acid, H<sub>2</sub>mal = malonic acid, H<sub>2</sub>suc = succinic acid), have been synthesized and structurally characterized. Complex **1** is a 3-D framework with a 4-connected diamond topology with the topological notation of 6<sup>6</sup>. Complex **2** exhibits 2-D layers with (6,3) networks. Complex **3** displays a 3-D framework constructed through unusual 2-D → 3-D parallel interpenetration of corrugated 2-D (6,3) networks. IR spectra, PXRD patterns, thermogravimetric curves, and photoluminescence spectra are addressed.

\*Corresponding author. Email: [mxr@zzu.edu.cn](mailto:mxr@zzu.edu.cn)

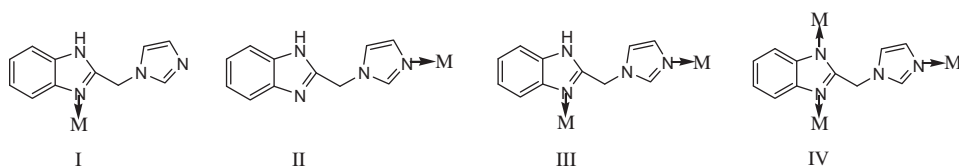
**Keywords:** Zn(II)-complex; 2-(1*H*-imidazolyl-1-ylmethyl)-1*H*-benzimidazole; Aliphatic dicarboxylates; Photoluminescence property; Thermostability

## 1. Introduction

Recently, we have focused our attention on the design and synthesis of metal-organic frameworks (MOFs) based on 2-(1*H*-imidazolyl-1-methyl)-1*H*-benzimidazole (imb), since, it has the following interesting advantages. First, it has three potential *N*-donors and can act as unidentate or bidentate bridging ligand in constructing complexes, and it may be deprotonated to coordinate to metal ion as a tridentate ligand (scheme 1). Second, it can act as both hydrogen bond acceptor and donor due to the presence of the amino group of benzimidazole ring and nitrogens of benzimidazole and imidazole rings. Third, it can offer tunability of structural frameworks owing to the presence of the methylene spacer. Twenty-three fascinating metal-organic complexes have been obtained using either one type of imb ligand or imb, and aromatic polycarboxylates [1–3]. Among the reported imb-based complexes, six complexes,  $[\text{CdCl}_2(\text{C}_{11}\text{H}_{10}\text{N}_4)_2(\text{H}_2\text{O})_2] \cdot 6\text{H}_2\text{O}$  [2] ( $\text{C}_{11}\text{H}_{10}\text{N}_4 = 1-[(1H\text{-benzimidazol-2-yl)methyl]-1H-imidazole}$ ),  $[\text{Cd}_2(\text{L})_4(\mu_2\text{-Cl})(\text{Cl})(\text{H}_2\text{O})]_n$ ,  $[\text{Cd}_2(\text{L})_4(\mu_2\text{-Br})(\text{Br})(\text{H}_2\text{O})]_n$  ( $\text{L} = 2-(1H\text{-imidazolyl-1-ylmethyl)-1H-benzoimidazole}$ ) [3(a)],  $[\text{Ni}(\text{C}_9\text{H}_5\text{O}_6)_2(\text{C}_{11}\text{H}_{10}\text{N}_4)_2] \cdot 8\text{H}_2\text{O}$  ( $\text{C}_9\text{H}_5\text{O}_6 = 3,5\text{-dicarboxybenzoate anion}$ ) [3(b)],  $\{[\text{Co}(\text{bdic})(\text{imb})_2(\text{H}_2\text{O})_2] \cdot 2\text{H}_2\text{O}\}_n$ , and  $\{[\text{Ni}(\text{bdic})(\text{imb})_2(\text{H}_2\text{O})_2] \cdot 2\text{H}_2\text{O}\}_n$  ( $\text{H}_2\text{dic} = 1,4\text{-benzenedicarboxylic acid}$ ) [3(c)], were prepared by Professors Wang, Jia, et al. and all the others are synthesized by our research group [1].

Among the 23 imb-based complexes, there is no complex based on imb and aliphatic dicarboxylates. As an extension of previous work, we introduced the flexible aliphatic dicarboxylates into the Zn(II)/imb system and studied the dicarboxylate induced variation of structures. Aliphatic dicarboxylate ligands play an important role in coordination chemistry, adopting diverse binding modes and geometrical configurations to provide unique MOFs [4]. Changes in the flexibility, length, extended direction, and angle of the spacer can lead to classes of complexes bearing diverse architectures and functions [5]. These ligands can act as hydrogen bond acceptors and donors to form or strengthen supramolecular structures or allow for guest structures by hydrogen bonding interactions, since aliphatic dicarboxylic acid can be partially or fully deprotonated [6]. Some discrete examples from small molecular aliphatic dicarboxylates such as oxalate [7], malonate [8], succinate [9], etc., have been reported.

In this work, we introduce different aliphatic dicarboxylic acid to the Zn/imb system, and three unusual complexes,  $[\text{Zn}(\text{ox})(\text{imb})]$  (**1**),  $[\text{Zn}_2(\text{mal})_2(\text{imb})_2]$  (**2**), and  $[\text{Zn}(\text{suc})(\text{imb})] \cdot \text{H}_2\text{O}$  (**3**), were obtained. In addition, IR spectra, powder X-ray diffraction (PXRD) patterns, thermostability, and fluorescence of **1–3** have been investigated.



Scheme 1. Potential coordination modes of imb.

## 2. Experimental

### 2.1. Materials and physical measurements

All reagents and solvents were commercially available except for imb which was synthesized according to the literature [10]. FT-IR spectra were recorded as KBr pellets from 400 to 4000  $\text{cm}^{-1}$  on a Bruker Tensor 27 spectrophotometer. Elemental analyses (C, H, and N) were carried out on a FLASH EA 1112 elemental analyzer. PXRD patterns were recorded using Cu-K $\alpha$ 1 radiation on a PANalytical X'Pert PRO diffractometer. Thermal analyses were performed on a Netzsch STA 449C thermal analyzer at room temperature at a heating rate of 10  $^{\circ}\text{C min}^{-1}$  in air. Luminescence spectra for powdered solid samples were measured at room temperature on a Hitachi 850 fluorescence spectrophotometer.

### 2.2. Synthesis of [Zn(ox)(imb)] (1)

A mixture of  $\text{Zn}(\text{NO}_3)_2 \cdot 6\text{H}_2\text{O}$  (0.1 mM), imb (0.1 mM), oxalic acid (0.1 mM), DMF (1 mL), and distilled water (8 mL) was sealed in a 25-mL Teflon-lined stainless steel container and heated at 120  $^{\circ}\text{C}$  for three days. After the mixture cooled to room temperature at a rate of 5  $^{\circ}\text{C/h}$ , colorless block crystals of **1** were obtained with a yield of 12.3 mg, 35% (based on Zn). Anal. Calcd for  $\text{C}_{13}\text{H}_{10}\text{N}_4\text{O}_4\text{Zn}$  (%): C, 44.40; H, 2.87; N, 15.94. Found: C, 44.02; H, 2.76; N, 16.28. IR (KBr,  $\text{cm}^{-1}$ ): 3132 (m), 1673 (s), 1606 (s), 1520 (s), 1495 (s), 1468 (s), 1450 (s), 1349 (s), 1283 (s), 1092 (s), 739 (s).

### 2.3. Synthesis of [Zn<sub>2</sub>(mal)<sub>2</sub>(imb)<sub>2</sub>] (2)

The same synthetic method as that for **1** was used except that oxalic acid was replaced by malonic acid (0.1 mM). Yield: 16.8 mg, 46% (based on Zn). Anal. Calcd for  $\text{C}_{28}\text{H}_{24}\text{N}_8\text{O}_8\text{Zn}_2$  (%): C, 45.98; H, 3.31; N, 15.33. Found: C, 45.63; H, 3.41; N, 15.67. IR (KBr,  $\text{cm}^{-1}$ ): 3129 (m), 1640 (s), 1616 (s), 1525 (m), 1495 (m), 1478 (s), 1453 (m), 1413 (s), 1361 (s), 1338 (s), 1289 (m), 1093 (m), 747 (s).

### 2.4. Synthesis of [Zn(suc)(imb)]·H<sub>2</sub>O (3) and [Zn(suc)(imb)] (3a)

The same synthetic method as that for **1** was used except that oxalic acid was replaced by succinic acid (0.1 mM). Yield: 25.8 mg, 65% (based on Zn). Anal. Calcd for  $\text{C}_{15}\text{H}_{16}\text{N}_4\text{O}_5\text{Zn}$  (%): C, 45.30; H, 4.06; N, 14.09. Found: C, 45.02; H, 4.15; N, 14.27. IR (KBr,  $\text{cm}^{-1}$ ): 3493 (s), 3138 (m), 1615 (s), 1524 (s), 1504 (m), 1471 (m), 1450 (m), 1420 (s), 1374 (s), 1285 (s), 1103 (m), 742 (s). Crystals of **3** were placed in an atmospheric pressure drying oven and heated to 250  $^{\circ}\text{C}$  for 6 h. Then crystals of **3a** were obtained and kept in a desiccator.

### 2.5. Crystal data collection and refinement

A suitable single crystal of each complex was carefully selected and glued to a thin glass fiber. Crystal structure determination by X-ray diffraction was performed on a Rigaku Saturn 724 CCD area detector with graphite monochromator for the X-ray source (Mo-K $\alpha$  radiation,  $\lambda = 0.71073 \text{ \AA}$ ) operating at 50 kV and 40 mA. The data were collected by  $\omega$  scan mode at 293(2) K; the crystal-to-detector distance was 45 mm. An

empirical absorption correction was applied. The data were corrected for Lorentz and polarization effects. The structures were solved by direct methods and refined by full-matrix least-squares and difference Fourier techniques, based on  $F^2$ , using SHELXS-97 [11]. All non-hydrogen atoms were refined anisotropically. The hydrogens bound to carbon and nitrogen were positioned geometrically and refined using a riding model. In **3**, there are two crystallographically independent halves of lattice water molecules (O5 and O6), for which O6 has a site occupancy of 0.5 and O5 is located on a twofold axis. The hydrogens of water molecules were found at reasonable positions in the difference Fourier map and located there. All hydrogens were included in the final refinement. Crystallographic parameters and structural refinement for the complexes are summarized in table 1. Selected bond lengths and angles of the complexes are listed in table 2. Hydrogen bonds are listed in table 3.

### 3. Results and discussion

#### 3.1. IR spectra

The absorption band at  $3493\text{ cm}^{-1}$  for **3** may be characteristic of lattice water [12]. Absorption bands at  $3129\text{--}3138\text{ cm}^{-1}$  may originate from the Ar–H stretch [1(d)]. The

Table 1. Crystal data and structure refinement data of **1–3**.

Complex	<b>1</b>	<b>2</b>	<b>3</b>
Formula	$\text{C}_{13}\text{H}_{10}\text{N}_4\text{O}_4\text{Zn}$	$\text{C}_{28}\text{H}_{24}\text{N}_8\text{O}_8\text{Zn}_2$	$\text{C}_{15}\text{H}_{16}\text{N}_4\text{O}_5\text{Zn}$
Formula weight	351.62	731.29	397.69
$T$ (K)	293(2)	293(2)	293(2)
Crystal system	Orthorhombic	Monoclinic	Orthorhombic
Space group	$Pna2(1)$	$P2(1)/c$	$Pbcn$
Unit cell dimensions ( $\text{\AA}$ , $^\circ$ )			
$a$ ( $\text{\AA}$ )	7.8287(16)	14.757(3)	12.702(3)
$b$ ( $\text{\AA}$ )	12.824(3)	14.094(3)	15.127(3)
$c$ ( $\text{\AA}$ )	13.415(3)	14.207(3)	17.401(4)
$\alpha$ ( $^\circ$ )	90	90	90
$\beta$ ( $^\circ$ )	90	101.59(3)	90
$\gamma$ ( $^\circ$ )	90	90	90
Volume ( $\text{\AA}^3$ )	1346.8(5)	2894.7(10)	3343.6(12)
$Z$	4	4	8
Calculated density ( $\text{Mg m}^{-3}$ )	1.734	1.678	1.580
Absorption coefficient ( $\text{mm}^{-1}$ )	1.849	1.724	1.503
$F(0\ 0\ 0)$	712	1488	1632
Crystal size ( $\text{mm}^3$ )	$0.18 \times 0.15 \times 0.11$	$0.18 \times 0.16 \times 0.12$	$0.19 \times 0.18 \times 0.15$
$\theta$ Range for data collection ( $^\circ$ )	2.20–27.87	2.02–25.50	2.09–25.50
$h$ range	$-10 \leq h \leq 9$	$-12 \leq h \leq 17$	$-15 \leq h \leq 15$
$k$ range	$-16 \leq k \leq 14$	$-12 \leq k \leq 17$	$-18 \leq k \leq 18$
$l$ range	$-17 \leq l \leq 17$	$-14 \leq l \leq 17$	$-20 \leq l \leq 21$
$R_{\text{int}}$	0.0457	0.0477	0.0447
Data/restraints/parameters	3190/1/199	5374/0/415	3109/0/231
Goodness-of-fit on $F^2$	1.096	1.080	1.268
Final $R$ indices [ $I > 2\sigma(I)$ ]	$R_1 = 0.0456$ $wR_2 = 0.0748$	$R_1 = 0.0582$ $wR_2 = 0.1212$	$R_1 = 0.0577$ $wR_2 = 0.1199$
$R$ indices (all data)	$R_1 = 0.0512$ $wR_2 = 0.0776$	$R_1 = 0.0828$ $wR_2 = 0.1349$	$R_1 = 0.0586$ $wR_2 = 0.1203$
$\Delta\rho_{\text{fin}}$ (max/min), $\text{e \AA}^{-3}$	0.372 and $-0.336$	0.770 and $-0.342$	0.669 and $-0.668$

Table 2. Selected bond lengths (Å) and angles (°) for 1–3 with estimated standard deviations in parentheses.

Complex 1			
Zn(1)–O(4)#1	2.042(3)	Zn(1)–O(1)	2.054(3)
Zn(1)–N(1)	2.080(3)	Zn(1)–N(3)#2	2.092(3)
Zn(1)–O(3)	2.140(3)	Zn(1)–O(2)#1	2.552(3)
O(4)#1–Zn(1)–O(1)	154.28(11)	O(4)#1–Zn(1)–N(1)	93.45(13)
O(1)–Zn(1)–N(1)	95.66(12)	O(4)#1–Zn(1)–N(3)#2	95.21(12)
O(1)–Zn(1)–N(3)#2	106.30(12)	N(1)–Zn(1)–N(3)#2	101.92(13)
O(4)#1–Zn(1)–O(3)	84.56(12)	O(1)–Zn(1)–O(3)	79.44(11)
N(1)–Zn(1)–O(3)	162.14(12)	N(3)#2–Zn(1)–O(3)	95.94(12)
O(4)#1–Zn(1)–O(2)#1	72.53(10)	O(1)–Zn(1)–O(2)#1	84.29(10)
N(1)–Zn(1)–O(2)#1	85.33(11)	N(3)#2–Zn(1)–O(2)#1	166.27(11)
O(3)–Zn(1)–O(2)#1	77.13(11)		
Complex 2			
Zn(1)–O(1)	1.954(3)	Zn(1)–N(4)#1	1.977(4)
Zn(1)–O(3)#2	1.988(3)	Zn(1)–N(1)	2.008(3)
Zn(2)–O(8)#3	1.970(3)	Zn(2)–O(5)	1.987(4)
Zn(2)–N(5)	2.023(4)	Zn(2)–N(7)#4	2.035(4)
Zn(2)–O(6)	2.555(5)		
O(1)–Zn(1)–N(4)#1	119.64(16)	O(1)–Zn(1)–O(3)#2	93.71(14)
N(4)#1–Zn(1)–O(3)#2	110.15(16)	O(1)–Zn(1)–N(1)	103.38(15)
N(4)#1–Zn(1)–N(1)	117.26(15)	O(3)#2–Zn(1)–N(1)	110.08(15)
O(8)#3–Zn(2)–O(5)	95.69(15)	O(8)#3–Zn(2)–N(5)	109.81(15)
O(5)–Zn(2)–N(5)	119.67(18)	O(8)#3–Zn(2)–N(7)#4	108.22(15)
O(5)–Zn(2)–N(7)#4	110.49(16)	N(5)–Zn(2)–N(7)#4	111.44(15)
O(8)#3–Zn(2)–O(6)	151.45(14)	O(5)–Zn(2)–O(6)	55.90(14)
N(5)–Zn(2)–O(6)	89.37(15)	N(7)#4–Zn(2)–O(6)	82.52(15)
Complex 3			
Zn(1)–O(4)#1	1.951(3)	Zn(1)–O(1)	1.995(3)
Zn(1)–N(4)#2	2.004(3)	Zn(1)–N(1)	2.024(3)
O(4)#1–Zn(1)–O(1)	98.34(11)	O(4)#1–Zn(1)–N(4)#2	118.01(14)
O(1)–Zn(1)–N(4)#2	106.12(13)	O(4)#1–Zn(1)–N(1)	108.19(13)
O(1)–Zn(1)–N(1)	110.42(12)	N(4)#2–Zn(1)–N(1)	114.42(13)

Note: Symmetry transformations used to generate equivalent atoms: For 1: #1  $x - 1/2, -y + 3/2, z$ , #2  $-x + 1, -y + 1, z - 1/2$ . For 2: #1  $-x + 1, -y + 1, -z$ , #2  $x, -y + 1/2, z - 1/2$ , #3  $x, -y + 3/2, z - 1/2$ , #4  $-x, -y + 2, -z$ . For 3: #1  $-x + 1/2, -y + 1/2, z + 1/2$ , #2  $-x, -y, -z + 1$ .

Table 3. Hydrogen bonds for 1–3.

D–H···A	$d(\text{D–H})$ (Å)	$d(\text{H···A})$ (Å)	$d(\text{D···A})$ (Å)	$(\text{D–H···A})$ (°)
Complex 1				
N(4)–H(4A)···O(2)#5	0.86	1.99	2.810(4)	158.0
Complex 2				
N(2)–H(2C)···O(7)#7	0.86	2.03	2.737(5)	139.1
N(2)–H(2C)···O(5)#7	0.86	2.30	2.948(5)	131.7
N(8)–H(8B)···O(3)#8	0.86	1.92	2.758(5)	164.9
Complex 3				
N(2)–H(2B)···O(1)#4	0.86	2.04	2.830(4)	153.0
O(5)–H(1 W)···O(6)	0.85	2.08	2.75(2)	135.0
O(6)–H(3 W)···O(2)	0.85	2.04	2.783(10)	145.2
O(6)–H(2 W)···O(3)#4	0.85	2.09	2.683(10)	126.3

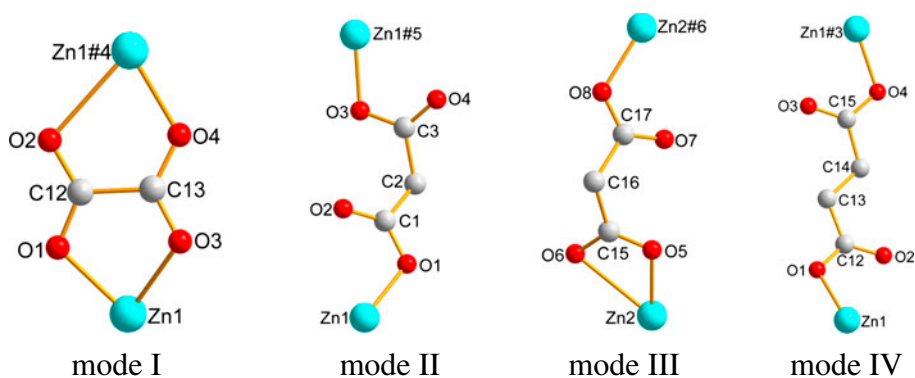
Note: Symmetry transformations used to generate equivalent atoms: For 1: #5  $x - 1, y, z$ . For 2: #7  $x + 1, y, z$ , #8  $-x + 1, y + 1/2, -z + 1/2$ . For 3: #4  $-x + 1/2, y - 1/2, z$ .

position of C=O absorption in the free carboxylic acid occurs at *ca.* 1760–1680  $\text{cm}^{-1}$ . Upon complexation to the metal center, this  $\nu(\text{C}=\text{O})$  band disappears and two new bands relating to the asymmetric  $\nu_a(\text{COO})$  and symmetric  $\nu_s(\text{COO})$  appear at 1673–1520  $\text{cm}^{-1}$  and 1468–1374  $\text{cm}^{-1}$ , respectively [13]. The absorption bands at 1606, 1520, and 1495  $\text{cm}^{-1}$  for **1**, 1616, 1525, 1495, and 1478  $\text{cm}^{-1}$  for **2**, and 1524, 1504, 1471, and 1450  $\text{cm}^{-1}$  for **3** may be due to stretching vibrations of  $\nu_{\text{C}=\text{C}}$  and  $\nu_{\text{C}=\text{N}}$ , and the absorption bands at 1283 and 1092  $\text{cm}^{-1}$  for **1**, 1289 and 1093  $\text{cm}^{-1}$  for **2**, and 1285 and 1103  $\text{cm}^{-1}$  for **3**, respectively, may be assigned to stretching vibrations of  $\nu_{\text{C}=\text{N}}$  and  $\nu_{\text{C}-\text{C}}$  [14]. The absorption bands at 739  $\text{cm}^{-1}$  for **1**, 747  $\text{cm}^{-1}$  for **2** and 742  $\text{cm}^{-1}$  for **3** may be characteristic of the stretching vibration of *o*-phenylene [15]. The IR data are consistent with the structures of **1–3**.

### 3.2. Crystal structure of [Zn(ox)(imb)] (**1**)

X-ray crystallographic analysis revealed that **1** crystallizes in the orthorhombic space group  $Pna2_1$  and has some intriguing features. The asymmetric unit contains one Zn (II), one  $\text{ox}^{2-}$ , and one imb ligand. As shown in table 2, Zn–O distances of 2.054(3)–2.140(3) Å and Zn–N distances of 2.080(3) Å and 2.092(3) Å are within the normal range [16(a–c)]. Although the Zn1–O2#1 distance of 2.552(3) Å is somewhat longer than the other three Zn–O distances, it is close to the Zn–O distances in  $[\text{Zn}_3(\text{L})(\text{BTC})_2(\text{H}_2\text{O})_2] \cdot 3\text{H}_2\text{O}$  (Zn–O: 2.557(4) Å, L = 1,2,4,5-tetrakis(imidazol-1-ylmethyl)benzene,  $\text{H}_3\text{BTC}$  = 1,3,5-benzenetricarboxylic acid) and  $[\text{Zn}(\text{pyip})(\text{glu})]_n$  (Zn–O: 2.550 Å,  $\text{pyip}$  = 2-(pyridin-3-yl)-1H-imidazo[4,5]-f[1,10]phenanthroline,  $\text{H}_2\text{glu}$  = glutaric acid) [16 (d, e)]. These suggest that there is a non-negligible interaction between Zn1 and O(2) #1. Hence, the Zn(II) center can be regarded as a distorted octahedral environment [figure 1(a)]. The equatorial plane of the distorted octahedron is composed of N1, O1, O3, and O4#1 while the axial positions are occupied by O2#1 and N3#2 with a O2#1–Zn1–N3#2 bond angle of 166.27(11)°.

As shown in figure 1(b), along the *c*-direction each imb links two Zn(II) ions to give 1-D chains and these chains are connected by  $\text{ox}^{2-}$  to form a 2-D undulating layer along the *bc* plane, which contain large hexagonal unit  $[\text{Zn}_6(\text{ox})_2(\text{imb})_4]$  with the six Zn(II) ions at the corners and two  $\text{ox}^{2-}$  anions and four imb ligands at the edges. In each  $[\text{Zn}_6(\text{ox})_2(\text{imb})_4]$  unit,



Scheme 2. The coordination modes of aliphatic dicarboxylates in **1–3**.

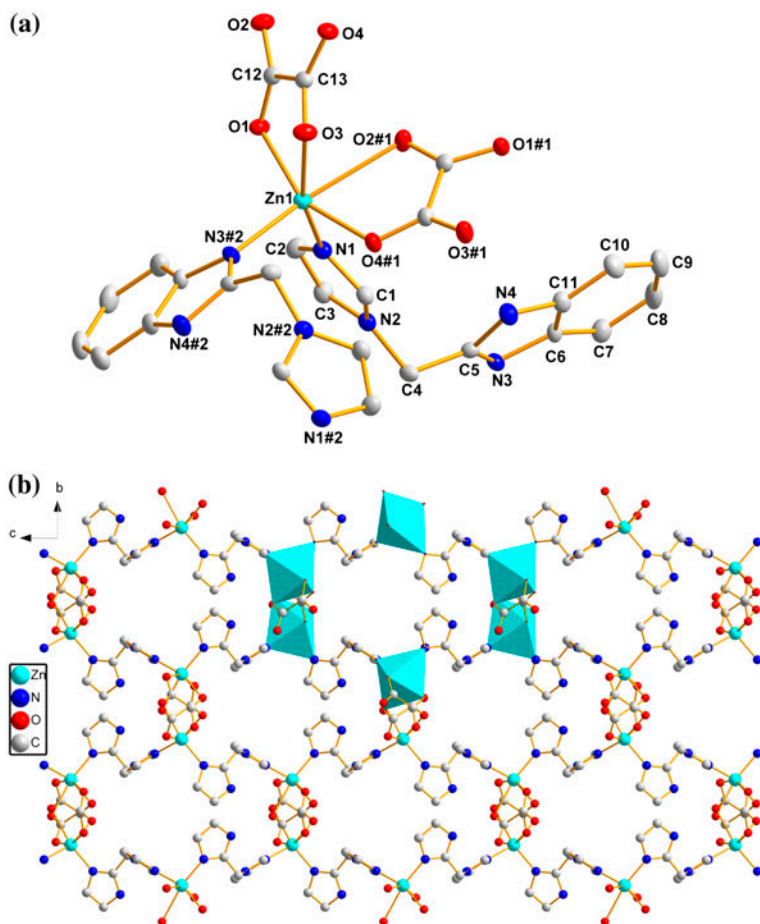


Figure 1. (a) Coordination environment of Zn(II) ion in **1**, showing 30% thermal ellipsoids; hydrogens are omitted for clarity (symmetry codes: #1  $x - 1/2, -y + 3/2, z$ ; #2  $-x + 1, -y + 1, z - 1/2$ ); (b) ball-and-stick view of the 2-D layer composed of the hexagonal unit  $[\text{Zn}_6(\text{ox})_2(\text{imb})_4]$  in **1**; benzene rings are omitted for clarity; (c) view of the 3-D structure of **1**; (d) 1-D···Zn-ox-Zn-ox···zigzag chain in **1**; parts of the imb ligand are omitted for clarity; and (e) 3-D network structure of **1** (color code: red stick, imb linker; turquoise stick, ox<sup>2-</sup> linker) (see <http://dx.doi.org/10.1080/00958972.2014.984702> for color version).

the Zn(II)–Zn(II) distance separated by ox<sup>2-</sup> is 5.5585(10) Å and the Zn(II)–Zn(II) distance separated by imb is 8.6488(15) Å. As for imb, the dihedral angle between the benzimidazole and imidazole rings is 69.2°. The ox<sup>2-</sup> is not planar and the two –CO<sub>2</sub> entities are twisted 11.5° with respect to each other around the C–C bond. Each ox<sup>2-</sup> connect to two Zn(II) centers with bis-bidentate coordination mode (O1 and O3 connect Zn1, O2 and O4 link Zn1#4) (scheme 2, mode I). The undulating 2-D layers are connected by ox<sup>2-</sup>, resulting in a 3-D framework [figure 1(c)]. Figure 1(d) gives the 1-D···Zn-ox-Zn-ox···zigzag chain along the *a*-direction. Insight into the nature of this intricate framework is provided by TOPOS analysis software [17], reducing multidimensional structures to simple nodes and connection nets.



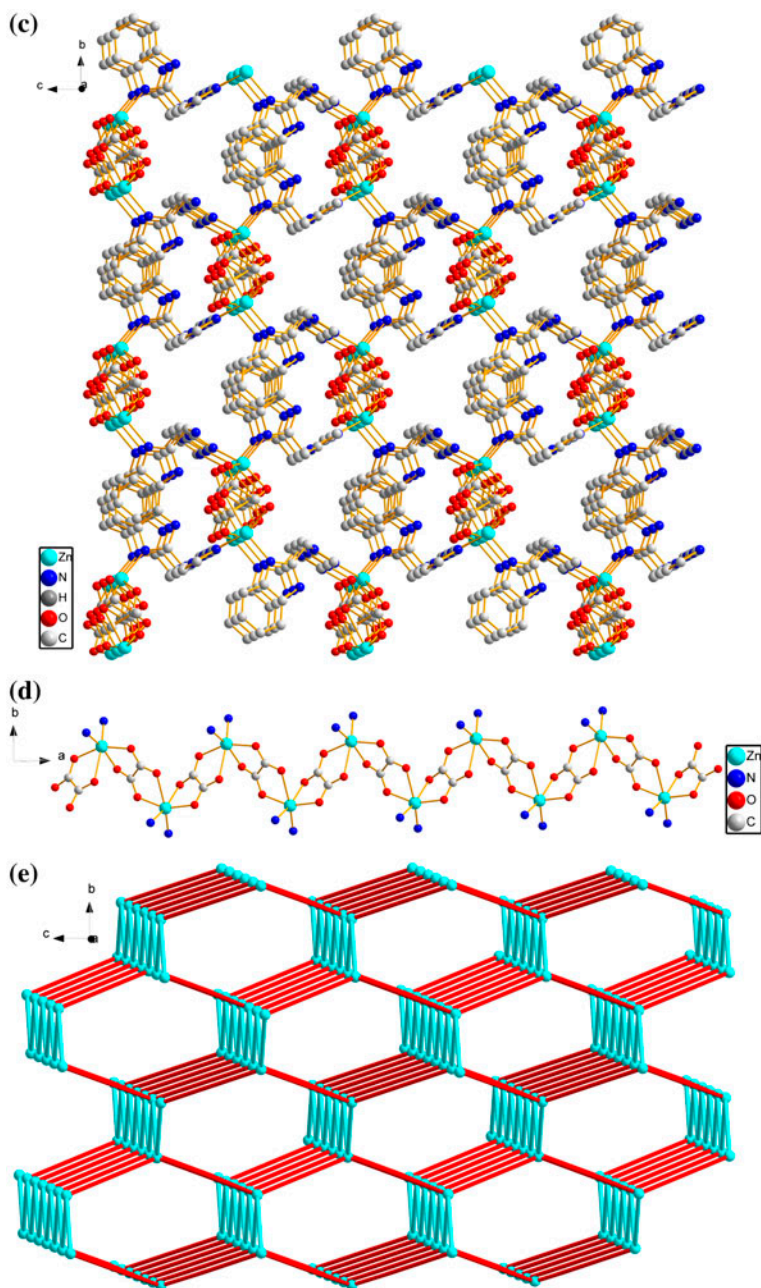


Figure 1. (Continued).

The Zn(II) ion can be regarded as a 4-connected node, the imb ligands and  $\text{ox}^{2-}$  anions are considered as linear linkers. Accordingly, the 3-D framework of **1** can be simplified to a 4-connected diamond topology with the topological notation of  $6^6$  [figure 1(e)].

### 3.3. Crystal structure of $[Zn_2(mal)_2(imb)_2]$ (**2**)

When  $H_2mal$  was utilized in place of  $H_2ox$  under similar synthetic conditions, **2** is isolated with a different structure than **1**. Complex **2** crystallizes in monoclinic space group  $P2_1/c$ , different from **1**. As shown in figure 2(a), the structure of **2** contains two crystallographically

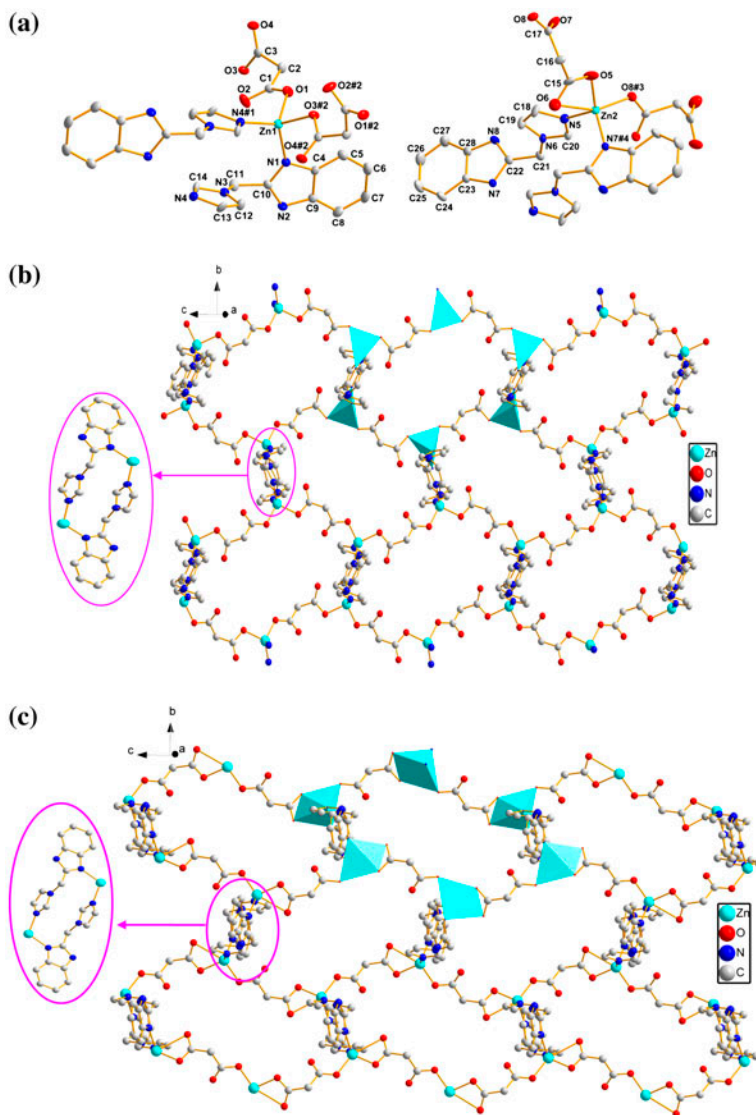


Figure 2. (a) Coordination environment of Zn(II) ion in **2**, showing 30% thermal ellipsoids; hydrogens are omitted for clarity (symmetry codes: #1  $-x + 1, -y + 1, -z$ ; #2  $x, -y + 1/2, z - 1/2$ ; #3  $x, -y + 3/2, z - 1/2$ ; #4  $-x, -y + 2, -z$ ); (b) ball-and-stick view of the 2-D layer of Zn1 composed of  $[Zn_6(mal)_4(imb)_4]$  in **2**; benzene rings are omitted for clarity; (c) ball-and-stick view of the 2-D layer of Zn2 composed of hexagonal  $[Zn_6(mal)_4(imb)_4]$  in **2**; benzene rings are omitted for clarity; (d) view of hydrogen bonds between adjacent layers (color code: turquoise, Zn1 layer; pink, Zn2 layer); and (e) schematic view of the packing mode of **2** in the solid state (color code: turquoise, Zn1 layers; pink, Zn2 layers) (see <http://dx.doi.org/10.1080/00958972.2014.984702> for color version).

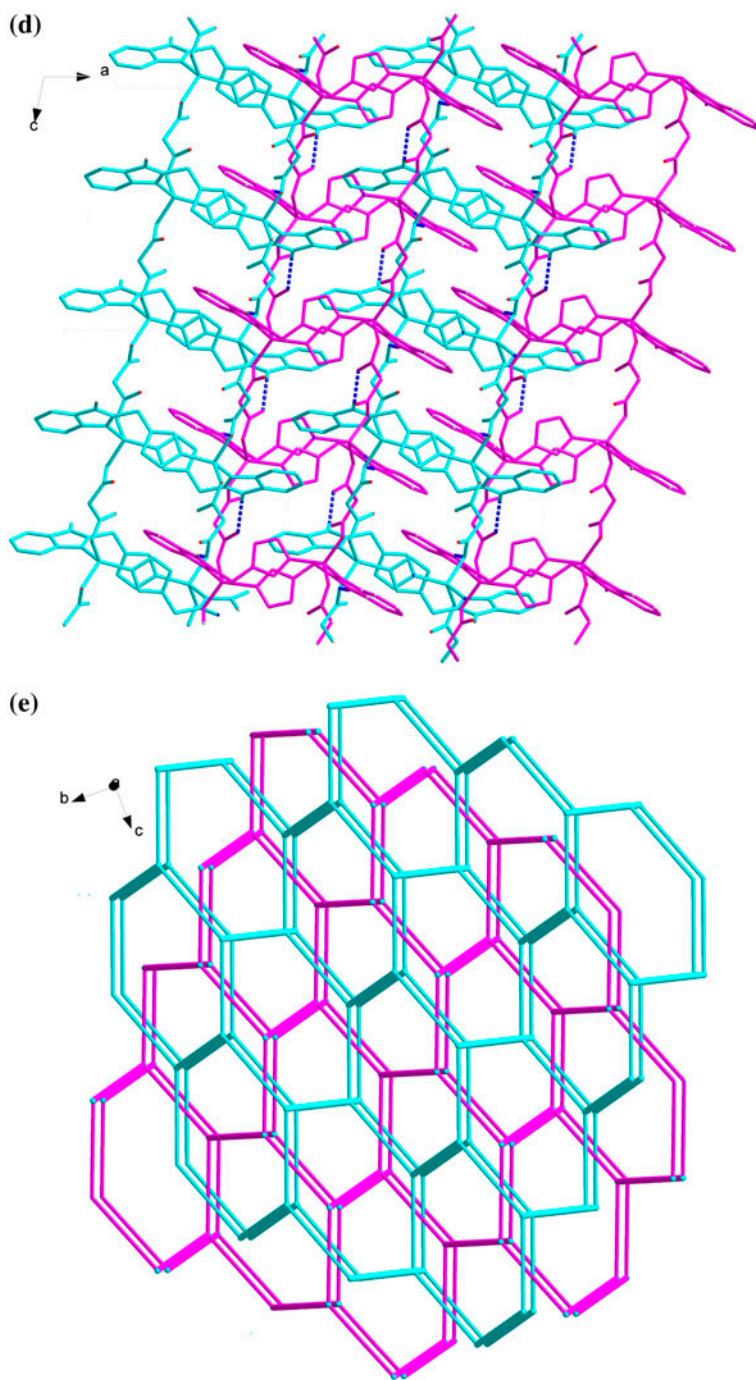


Figure 2. (Continued).

distinct Zn(II) ions (Zn1 and Zn2) with different coordination environments, two crystallographically distinct imb molecules with different conformations, and two crystallographically distinct mal<sup>2-</sup> anions with different coordination modes. Zn1 shows a tetrahedral environment of two nitrogens from imidazole and benzimidazole rings of two symmetry-related imb ligands and two oxygens from two symmetry-related mal<sup>2-</sup> anions. The Zn1–O (1.954(3), 1.987(4) Å) and Zn1–N (1.977(4), 2.035(4) Å) bond lengths are close to those observed in **1**. For each imb coordinating to Zn1, the dihedral angle between the benzimidazole and imidazole rings is 97.8°. For each mal<sup>2-</sup> coordinating to Zn1 ions, the two carboxylate groups are tilted 61.3°. This distortion can be attributed to more restrictive requirements of the molecular interactions. As shown in figure 2(b), a pair of imb ligands bind two Zn1 ions simultaneously through their imidazole N and benzimidazole N forming a dinuclear unit [(Zn1)<sub>2</sub>(imb)<sub>2</sub>]. The mal<sup>2-</sup> anions bridge through monodentate carboxyl groups (O1 coordinates to Zn1 and O3 coordinates to Zn1#5) (scheme 2, mode II). Each Zn1, in turn, is connected to two imb ligands and two mal<sup>2-</sup> anions to form an infinite 2-D (6,3) network (named type A) along the *bc* plane. These 2-D layers are composed of [(Zn1)<sub>6</sub>(mal)<sub>4</sub>(imb)<sub>4</sub>] large hexagonal units, and all of the Zn1 ions, imb ligands, and mal<sup>2-</sup> anions in each layer are equivalent. The composition of the hexagonal unit in **2** is different from that in **1**. For each hexagonal unit in **2**, four mal<sup>2-</sup> anions are the four edges with length of 7.6103(16) Å and two pairs of imb ligands are the other two edges with length of 6.8322(14) Å, and six Zn(II) ions represent the six vertices. While the hexagonal [Zn<sub>6</sub>(ox)<sub>2</sub>(imb)<sub>4</sub>] in **1** is composed of two ox<sup>2-</sup> anions, four imb ligands, and six Zn(II) ions. Similar to the Zn1–O2#1 bond length in **1**, the Zn2–O6 bond length of 2.555(5) Å in **2** is also a non-negligible interaction between Zn2 and O6. So Zn2 is located in an irregular ZnO<sub>3</sub>N<sub>2</sub> coordination environment [figure 2(a)] and coordinated by two nitrogens from two symmetry-related imb ligands and three oxygens from two symmetry-related mal<sup>2-</sup> anions. As shown in table 2, the Zn2–O and Zn2–N bond lengths are close to the Zn1–O and Zn1–N bond lengths in **1**. For each imb coordinating to Zn2, the dihedral angle between the benzimidazole and imidazole rings is 80.2°. Furthermore, two carboxylates of each mal<sup>2-</sup> coordinating to Zn2 display different coordination modes, one is bidentate chelating and the other is monodentate (O5 and O6 coordinate to Zn2 with chelating mode, O8 coordinates to Zn2#6) (scheme 2, mode III), while both carboxylates of each mal<sup>2-</sup> are monodentate to Zn1. For each mal<sup>2-</sup> coordinating to Zn2, the two carboxylate groups are tilted 59.3°. Like layer A, a pair of imb ligands bind two Zn2 ions simultaneously forming a dinuclear unit [(Zn2)<sub>2</sub>(imb)<sub>2</sub>], as depicted in figure 2(c). Each Zn2 is connected to two imb ligands and two mal<sup>2-</sup> anions to form an infinite 2-D (6,3) network (named type B) along the *bc* plane. These 2-D layers are composed of large hexagonal [(Zn2)<sub>6</sub>(mal)<sub>4</sub>(imb)<sub>4</sub>] units, and all of the Zn2 ions, imb ligands, and mal<sup>2-</sup> anions in each layer are equivalent. For each hexagonal unit, four mal<sup>2-</sup> anions are the four edges with the length of 7.5595(16) Å and two pairs of imb ligands are the other two edges with the length of 7.4021(14) Å; six Zn2 ions represent the six vertices.

In **2**, the imb molecules are bridging ligands and also hydrogen bond donors forming strong N–H···O hydrogen bonds with mal<sup>2-</sup> of adjacent layers [figure 2(d)]. As a result, along the *a*-direction, the above two kinds of 2-D layers are further connected in ABAB fashion through strong non-covalent hydrogen bonding interactions to form an overall 3-D structure. Figure 2(e) describes the simplified supramolecular structure of **2**.



### 3.4. Crystal structure of [Zn(suc)(imb)]·H<sub>2</sub>O (**3**)

Complex **3** crystallizes in orthorhombic space group *Pbcn*. The asymmetric unit contains one four-coordinate Zn(II), one imb, one succinate, and two crystallographically independent halves of lattice water molecules. Each Zn(II) ion has a distorted tetrahedral environment defined by two oxygens from two symmetry-related suc<sup>2-</sup> anions and two nitrogens from imidazole and benzimidazole rings of two symmetry-related imb ligands, as depicted in figure 3(a). The Zn–O (1.951(3), 1.995(3) Å) and Zn–N (2.004(3), 2.024(3) Å) bond lengths are close to those observed in **1** and **2**. For each imb, the dihedral angle between the benzimidazole and imidazole rings is 92.7°. For each suc<sup>2-</sup>, the dihedral angle between the planes defined by the carboxyl groups of each suc<sup>2-</sup> is 17.0°. Similar to **2**, a pair of imb ligands bind two Zn(II) ions simultaneously through their imidazole N and benzimidazole N forming a dinuclear [Zn<sub>2</sub>(imb)<sub>2</sub>] [figure 3(b)]. The Zn–Zn distance separated by imb ligands is 7.1351(13) Å, different from those in **1** and **2**. The suc<sup>2-</sup> anions exist in an *anti* conformation with a torsion angle (C12–C13–C14–C15) of –164.5(5)° and bridge through monodentate carboxylate groups (O1 coordinates to Zn1 and O4 coordinates to Zn1#3) (scheme 2, mode IV), which is the same as mal<sup>2-</sup> coordinating to Zn1 in **2**. The Zn–Zn distance of 9.1462(20) Å separated by suc<sup>2-</sup> is longer than those in **1** (Zn–Zn distance: 5.5585 (10) Å) and **2** (Zn–Zn distance: 7.6103(16) Å or 7.5595(16) Å). This suggests that the Zn–Zn distance is proportional to the length of the alkyl chain in aliphatic  $\alpha,\omega$ -dicarboxylates; the longer the alkyl chain, the longer the distance between zinc ions. Each Zn(II) is connected to two imb ligands and two suc<sup>2-</sup> anions to form an infinite 2-D (6,3) network along the *bc* plane, which contain large hexagonal [Zn<sub>6</sub>(suc)<sub>4</sub>(imb)<sub>4</sub>]. Like **2**, four suc<sup>2-</sup> anions are the four edges, two pairs of imb ligands are the other two edges, and six Zn(II) ions represent the six vertices. The potential guest accessible area in **3** is about 6.3% of unit cell volume, as calculated by PLATON [18]. The rest of the voids are large enough to be filled via mutual interpenetration of an independent equivalent framework, generating a twofold interpenetrating architecture.

Packing of the layers generates two sets of layers oriented toward the [1, 1, 0] and [1, –1, 0] directions, respectively. These two sets of layers catenate to each other in a parallel–parallel [19] arrangement to form a 2-D → 3-D inclined polycatenation structure [figure 3(c)]. The angle between these two sets of layers is 90°. The distance between adjacent layers of one set is *ca.* 9.7 Å. Further insight into one window of a layer shows that each window is catenated with two other windows from one layer in the other set. This parallel/parallel inclined polycatenation is somewhat exceptional, although the (6,3) network is rather common [20]. For example, Cao and co-workers reported a 2-D → 3-D inclined polycatenation complex [Cd(BPMP)(DCA)<sub>2</sub>(H<sub>2</sub>O)] based on a (4,4) network (BPMP = *N,N'*-bis-(4-pyridyl)-methyl)piperazine, DCA<sup>-</sup> = dicyanamide) [19(d)].

From the above discussion, the structural diversification of the three complexes should be ascribed to different coordination of the aliphatic dicarboxylate ligands and different distances between the two carboxylate groups in each aliphatic dicarboxylate ligand. For **1**, Zn(II) ions are bridged by imb ligands and semirigid ox<sup>2-</sup> anions with  $\mu_2\text{-}\eta^1\text{-}\eta^1\text{-}\eta^1\text{-}\eta^1$  mode leading to a 3-D framework. In **2**, mal<sup>2-</sup> anions show two different coordination modes:  $\mu_2\text{-}\eta^1\text{-}\eta^1$  and  $\mu_2\text{-}\eta^1\text{-}\eta^1\text{-}\eta^1$  bridging modes and the distances between the two carboxylate groups in mal<sup>2-</sup> anions are longer than with ox<sup>2-</sup>. Zn(II) ions are linked by imb ligands and mal<sup>2-</sup> anions to afford two kinds of 2-D layers. In each layer, six Zn(II) ions are linked by four mal<sup>2-</sup> anions and two pairs of imb ligands to form a hexagonal ring of approximate dimensions 16.0 × 11.1 Å or 17.9 × 11.3 Å. The dimensions of the cavity are not large

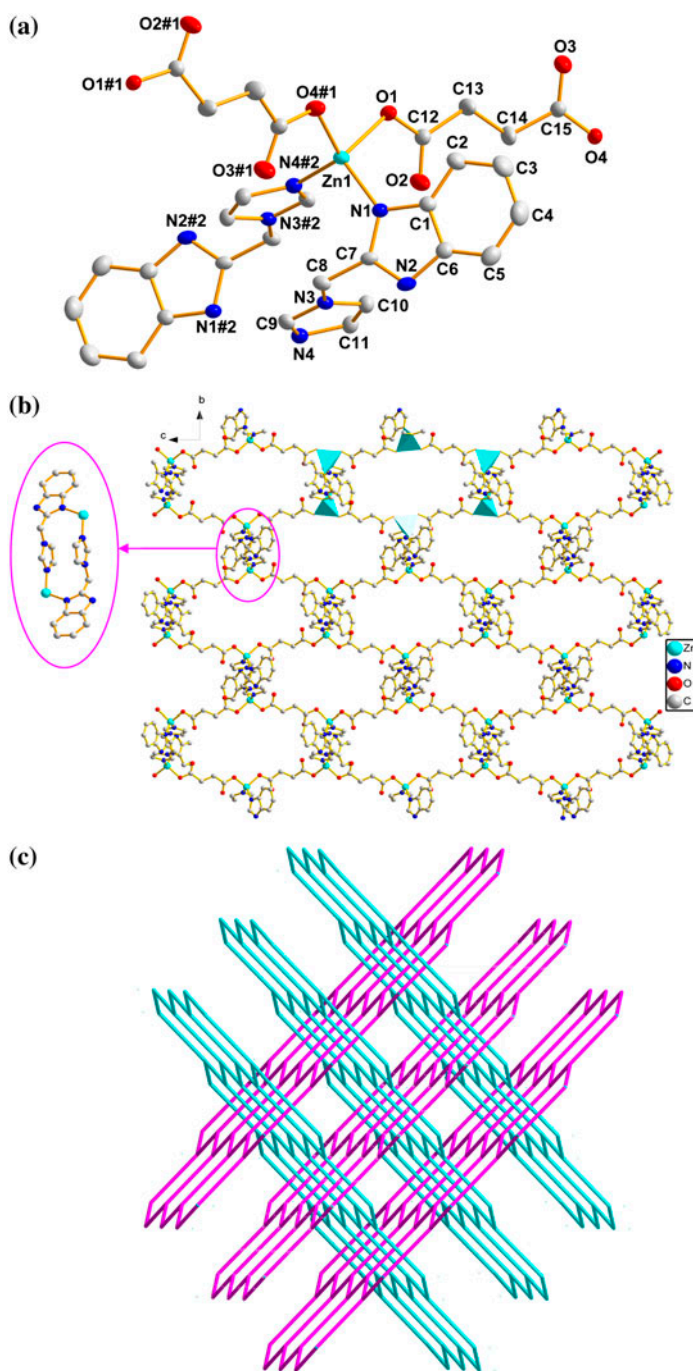


Figure 3. (a) Coordination environments of Zn(II) ion in **3**, showing 30% thermal ellipsoids; hydrogens and lattice water molecules are omitted for clarity (symmetry codes: #1 -  $x + 1/2$ ,  $-y + 1/2$ ,  $z + 1/2$ ; #2 -  $x$ ,  $-y$ ,  $-z + 1$ ); (b) ball-and-stick view of the 2-D layer composed of hexagonal  $[\text{Zn}_6(\text{suc})_4(\text{imb})_4]$  in **3**; and (c) schematic representation of the 2-D  $\rightarrow$  3-D interpenetrating nets in **3**.

enough to accommodate another net, and it allows an understanding of why **2** does not exhibit an interpenetrating structure. As a result, two kinds of 2-D layers are parallel stacked in ABAB fashion along the crystallographic *a*-axis and cross-linked by weak hydrogen bonding interactions between neighboring layers, which sustains the overall 3-D supra-molecular architecture. In **3**,  $\text{suc}^{2-}$  anions display  $\mu_2\text{-}\eta^1\text{-}\eta^1$  bridging mode and the distance between the two carboxylate groups in  $\text{suc}^{2-}$  is longer than that in  $\text{mal}^{2-}$  or  $\text{ox}^{2-}$ . Zn(II) ions are linked by imb ligands and  $\text{suc}^{2-}$  anions resulting in a 2-D structure. In each sheet, six Zn(II) ions are linked by four  $\text{suc}^{2-}$  anions and two pairs of imb ligands leading to a hexagonal cavity of approximate dimensions  $19.2 \times 12.7 \text{ \AA}$  which is large enough to accommodate another net. The 2-D layers catenate to each other in a parallel-parallel arrangement to form a 2-D  $\rightarrow$  3-D inclined polycatenation structure. Various framework structures can be achieved by choice of the aliphatic  $\alpha,\omega$ -dicarboxylate.

### 3.5. PXRD patterns and thermogravimetric analyses

To confirm that the crystal structures are truly representative of the bulk materials, PXRD experiments were carried out for **1–3** and **3a**. As shown in figure 4, the experimental PXRD patterns correspond well with the results simulated from the single crystal data, indicating the high purity of the synthesized samples, and single phases of **1–3** are formed. In addition, figure 4(c) also shows that the PXRD pattern of **3a** remains unchanged compared with the experimental PXRD pattern of **3**, indicating that the framework of **3** is stable after loss of lattice water molecules.

To characterize thermal stabilities of complexes, thermal gravimetric analyses (TGA) of **1–3** and **3a** were measured from 30 to 800 °C in air. Results of the TGA curves show that the three complexes possess different thermal stabilities (figure 5). For **1**, no obvious weight loss was observed until 371 °C, where the framework of the structure began to collapse. A weight loss of 24.93% from 371 to 419 °C was consistent with decomposition of oxalate anions (calculated 25.03%), and then successive pyrolysis continued to 656 °C, corresponding to decomposition of the imb ligands (observed 51.73%, calculated 51.83%). The final residue of 23.37% is ZnO (calculated 23.14%). Similar to the TG curve of **1**, **2** was stable to 312 °C and then lost weight from 312 to 428 °C corresponding to decomposition of malonate (observed 27.76%, calculated 27.98%). After 428 °C, further weight loss of 50.11% was assigned to the decomposition of imb ligands (calculated 49.76%) and then a white residue of ZnO (observed 22.13%, calculated 22.26%) remained. The TG curve for **3** shows the initial weight loss from 43 to 183 °C, which can be ascribed to removal of lattice water molecules (observed 4.38%, calculated 4.52%). The overall framework of **3** begins to collapse at 312 °C, and the ZnO residue of 20.40% (calculated 20.46%) is observed at 651 °C. Furthermore, the thermo-gravimetric analysis curve of **3a** shows that it was stable to 316 °C and then lost weight from 316 to 598 °C corresponding to decomposition of succinate anions and imb ligands. A white residue of ZnO (observed 21.58%, calculated 21.43%) remained.

### 3.6. Photoluminescence properties

Metal complexes ( $d^{10}$ ) with conjugated molecules as well as ancillary ligands are candidates for fluorescent properties and potential applications as fluorescent emitting materials [4(c), 9(a)]. The photoluminescence properties of **1–3** were investigated in the solid state at room temperature (figure 6). Complex **1** exhibits a photoluminescent peak with a maximum at

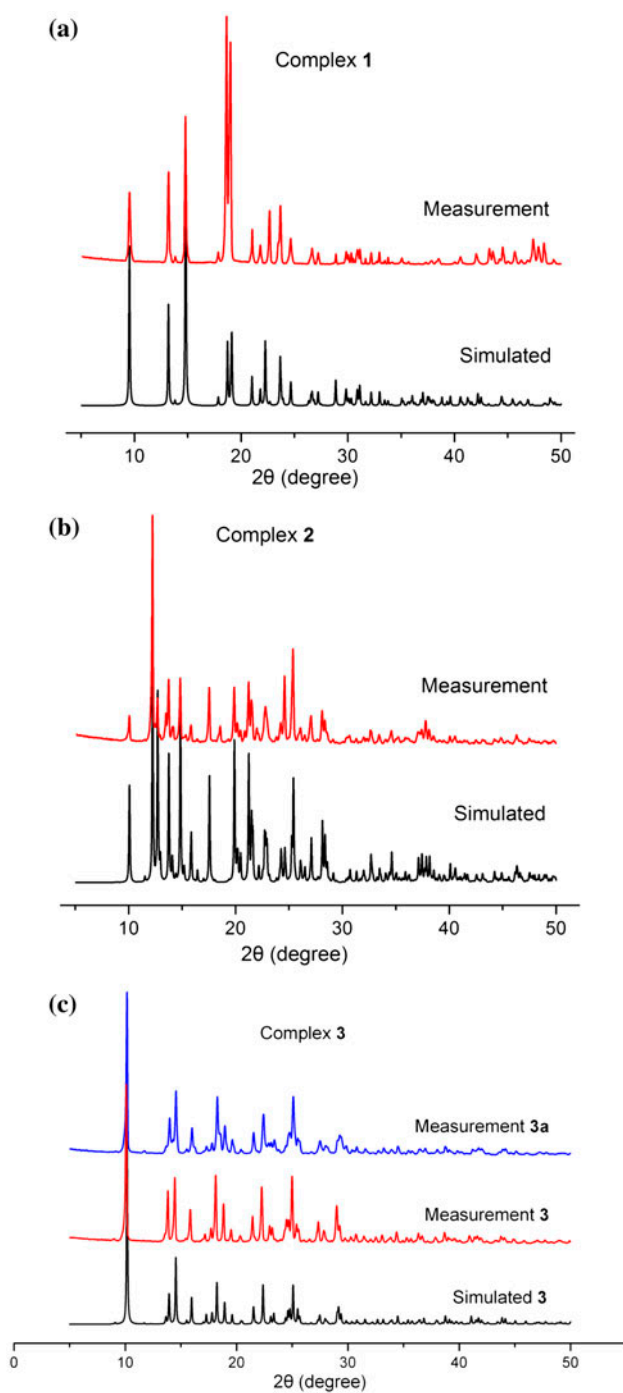


Figure 4. (a) The PXR D patterns of **1** at room temperature; (b) the PXR D patterns of **2** at room temperature; and (c) the PXR D patterns of **3** and **3a** (simulated patterns are generated from single-crystal diffraction data of **3**).



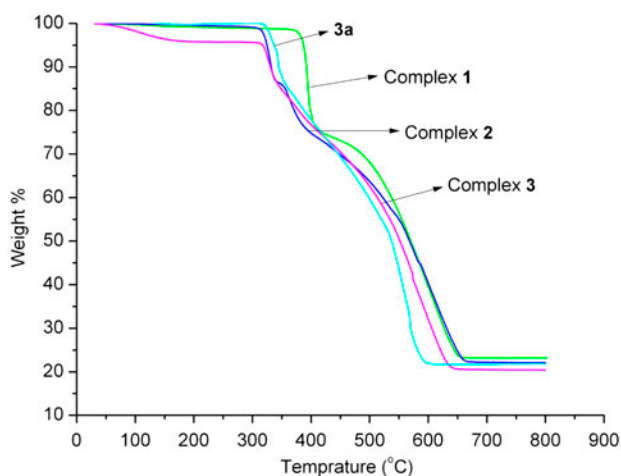


Figure 5. TG curves for 1–3 and 3a.

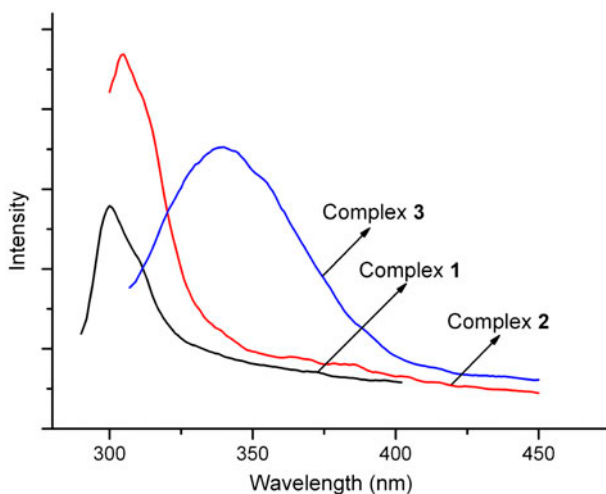


Figure 6. Photoluminescence properties of 1–3.

300 nm upon excitation at 286 nm, **2** shows an emission maximum band at 304 nm upon excitation at 287 nm, and **3** displays an emission with a maximum at 339 nm when excited at 296 nm. To understand the nature of the emission spectra, the luminescence properties of the free ligands under the same experimental conditions were recorded for comparison. As shown in figure S4 (see online supplemental material at <http://dx.doi.org/10.1080/00958972.2014.984702>), free imb displays strong photoluminescence with emission maxima at 303 nm ( $\lambda_{\text{ex}} = 270$  nm),  $\text{H}_2\text{ox}$  exhibits very weak photoluminescence with emission maxima at 343 nm ( $\lambda_{\text{ex}} = 286$  nm), and both  $\text{H}_2\text{mal}$  and  $\text{H}_2\text{suc}$  are nearly non-fluorescent from 280 to 500 nm at ambient temperature. Thus, the emissions of free aliphatic dicarboxylic acids  $\text{H}_2\text{ox}$ ,  $\text{H}_2\text{mal}$ , and  $\text{H}_2\text{suc}$  are very weak compared to that of free imb, so the aliphatic

dicarboxylic acids have almost no contribution to the fluorescent emissions of the synthesized complexes; similar cases have been reported [9(c), 21]. The emission peaks of **1** and **2** are essentially the same as the photoluminescent peak of imb, which indicates that the emission bands of **1** and **2** are intraligand transitions (LLCT) [21(c)]. In contrast to free imb, **3** shows slightly red-shifted emission bands caused by the metal–ligand coordination interactions which influence the rigidity and asymmetry of the ligands and the coordination environment of the metal centers [9(a, b)].

#### 4. Conclusion

We have synthesized three complexes under solvothermal condition using  $\text{Zn}(\text{NO}_3)_2 \cdot 6\text{H}_2\text{O}$  and imb in the presence of aliphatic dicarboxylic acid ( $\text{H}_2\text{ox}$ ,  $\text{H}_2\text{mal}$  or  $\text{H}_2\text{suc}$ ). These results illustrate that the final architectures of the complexes can be partially controlled by modifying the aliphatic dicarboxylic acids. Complex **1** is a 3-D structure which can be simplified to a topology with the topological notation of  $6^6$ . In **2**, Zn(II) ions are linked by imb and malonate ligands to 2-D layers containing (6,3) networks, and the layers are further stacked by hydrogen bonds to a 3-D structure. In **3**, the two sets of layers with (6,3) networks catenate to each other to form a 2-D  $\rightarrow$  3-D inclined polycatenation structure. It is expected the integration of aliphatic dicarboxylates and *N*-containing ligands may offer new opportunities to construct intriguing frames. We will continue to synthesize complexes based on mix-ligands of imb and aliphatic carboxylates and further investigate the influence of the spacer length, the conformations, and coordination modes of aliphatic  $\alpha,\omega$ -dicarboxylates on the complex structures.

#### Supplementary material

Crystallographic data for the structures in the form of CIF files have been deposited with the Cambridge Crystallographic Data Center as supplementary publication Nos. CCDC 950709–950711 for **1–3**, respectively. This data can be obtained free of charge via <http://www.ccdc.cam.ac.uk/conts/retrieving.html> (or from the Cambridge Crystallographic Data Center, 12 Union Road, Cambridge CB2 1EZ, UK; Fax: +44 1223 336 033).

#### Funding

We gratefully acknowledge the financial support by the National Natural Science Foundation of China [grant number J1210060].

#### References

- [1] (a) T. Li, X. Su, Y. Xiu, X.R. Meng. *J. Coord. Chem.*, **65**, 1792 (2012); (b) X. Su, T. Li, Y. Xiu, X.R. Meng. *Z. Naturforsch.*, **67b**, 678 (2012); (c) S.X. Yan, G.H. Jin, Y. Yang, X. Su, X.R. Meng. *Synth. React. Inorg. Met.-Org. Chem.*, **42**, 678 (2012); (d) S.X. Yan, D. Zhao, T. Li, R. Wang, X.R. Meng. *J. Coord. Chem.*, **65**, 945 (2012); (e) L. Zhao, B.T. Liu, T. Li, X.R. Meng. *Acta Cryst.*, **E68**, m162 (2012); (f) B.T. Liu, L. Zhao, T. Li, X.R. Meng. *Acta Cryst.*, **E67**, m1901 (2011); (g) X.X. Wang, X. Han, Y. Yang, X.R. Meng. *Synth. React. Inorg. Met.-Org. Chem.*, **44**, 462 (2014); (h) T. Li, R. Wang, X. Su, X.R. Meng. *Synth. React. Inorg. Met.-Org. Chem.*, **43**, 1452 (2013); (i) Z.W. Wang, M. Yu, T. Li, X.R. Meng. *J. Coord. Chem.*, **66**, 4163 (2013).

- [2] X.N. Xie, M. Lu, J. Yuan, H.X. Yang. *Acta Cryst.*, **E68**, m754 (2012).
- [3] (a) Y.T. Wang, G.M. Tang, Y.Q. Wei, T.X. Qin, T.D. Li, C. He, J.B. Ling, X.F. Long, S.W. Ng. *Cryst. Growth Des.*, **10**, 25 (2010); (b) Y.Y. Jia, J.J. Fan, X.G. Yin, W.L. Zhao. *Acta Cryst.*, **E69**, m184 (2013); (c) Y. Wang, S.X. Yan, Y.Z. Zhang, L.N. Sun, Z.H. Wei. *Z. Naturforsch.*, **68b**, 1225 (2013).
- [4] (a) L.F. Ma, L.Y. Wang, D.H. Lu, S.R. Batten, J.G. Wang. *Cryst. Growth Des.*, **9**, 1741 (2009); (b) S.N. Wang, J.F. Bai, Y.Z. Li, Y. Pan, M. Scheer, X.Z. You. *CrystEngComm*, **9**, 1084 (2007); (c) M. Du, C.P. Li, X.J. Zhao, Q. Yu. *CrystEngComm*, **9**, 1011 (2007); (d) S.K. Ghosh, P.K. Bharadwaj. *Inorg. Chem.*, **43**, 6887 (2004); (e) S.R. Batten, R. Robson. *Angew. Chem., Int. Ed.*, **37**, 1460 (1998).
- [5] (a) B.H. Ye, B.B. Ding, Y.Q. Weng, X.M. Chen. *Cryst. Growth Des.*, **5**, 801 (2005); (b) T. Düren, Y.S. Baeb, R.Q. Snurr. *Chem. Soc. Rev.*, **38**, 1237 (2009); (c) J.R. Li, A.A. Yakovenko, W. Lu, D.J. Timmons, W. Zhuang, D. Yuan, H.C. Zhou. *J. Am. Chem. Soc.*, **132**, 17599 (2010); (d) K.M. Blake, L.L. Johnston, J.H. Nettleman, R.M. Supkowski, R.L. LaDuca. *CrystEngComm*, **12**, 1927 (2010).
- [6] F. Oscar, P. Jorge, C.D. Laura, S.D. Fernando, L. Ana, L. Francesc, J. Miguel, R.P. Catalina. *Cryst. Growth Des.*, **8**, 3984 (2008).
- [7] D. Armentano, G.D. Munno, T.F. Mastropietro, M. Julve, F. Lloret. *J. Am. Chem. Soc.*, **127**, 10778 (2005); (b) D. Armentano, T.F. Mastropietro, G.D. Munno, P. Rossi, F. Lloret, M. Julve. *Inorg. Chem.*, **47**, 3772 (2008); (c) U. García-Couceiro, O. Castillo, A. Luque, J.P. García-Terán, G. Beobide, P. Román. *Cryst. Growth Des.*, **6**, 1839 (2006).
- [8] (a) Y. Rodríguez-Martín, M. Hernández-Molina, J. Sanchiz, C. Ruiz-Pérez, F. Lloret, M. Julve. *Dalton Trans.*, 2359, (2003); (b) F.S. Delgado, F. Lahoz, F. Lloret, M. Julve, C. Ruiz-Pérez. *Cryst. Growth Des.*, **8**, 3219 (2008); (c) F.S. Delgado, J. Sanchiz, C. Ruiz-Pérez, F. Lloret, M. Julve. *Inorg. Chem.*, **42**, 5938 (2003).
- [9] (a) G.L. Wen, Y.Y. Wang, W.H. Zhang, C. Ren, R.T. Liu, Q.Z. Shi. *CrystEngComm*, **12**, 1238 (2010); (b) C.Y. Xu, Q.Q. Guo, X.J. Wang, H.W. Hou, Y.T. Fan. *Cryst. Growth Des.*, **11**, 1869 (2011); (c) H. Ren, T.Y. Song, D.W. Lou, L.R. Zhang, Y.L. Chen, P. Zhang, J.N. Xu. *Inorg. Chim. Acta*, **373**, 79 (2011); (d) A.B. Caballero, A. Rodríguez-Diéguez, L. Lezama, J.M. Salas. *Cryst. Growth Des.*, **12**, 3583 (2012).
- [10] A.R. Katritzky, M. Drewniak-Deyrup, X.F. Lan, F. Brunner. *J. Heterocycl. Chem.*, **26**, 829 (1989).
- [11] G.M. Sheldrick. *Acta Crystallogr.*, **A64**, 112 (2008).
- [12] X. Han, X.X. Wang, G.H. Jin, X.R. Meng. *J. Coord. Chem.*, **66**, 800 (2013).
- [13] K. Nakamoto. *Infrared and Raman Spectra of Inorganic and Coordination Compounds, Part B*, 6th Edn, Wiley, Hoboken, New Jersey (2009).
- [14] A. Majumder, V. Gramlich, G.M. Rosair, S.R. Batten, J.D. Masuda, M.S.E. Fallah, J. Ribas, J.P. Sutter, C. Desplanches, S. Mitra. *Cryst. Growth Des.*, **6**, 2355 (2006).
- [15] X.R. Meng, W. Zhou, Y.F. Qi, H.W. Hou, Y.T. Fan. *J. Organomet. Chem.*, **695**, 766 (2010).
- [16] (a) D. Zhao, Y. Xiu, X.L. Zhou, X.R. Meng. *J. Coord. Chem.*, **65**, 112 (2012); (b) S.W. Jin, D.Q. Wang, Y.C. Xu. *J. Coord. Chem.*, **65**, 1953 (2012); (c) D. Deng, P. Liu, W. Fu, L. Li, F. Yang, B. Ji. *Inorg. Chim. Acta*, **363**, 891 (2010); (d) L. Gou, Z.X. Han, H.M. Hu, Q.R. Wu, X.L. Yang, Z.H. Yang, B.C. Wang, F. Wang, M.L. Yang, G.L. Xue. *Inorg. Chim. Acta*, **363**, 2590 (2010); (e) Q. Hua, Y. Zhao, G.C. Xu, M.S. Chen, Z. Su, K. Cai, W.Y. Sun. *Cryst. Growth Des.*, **10**, 2553 (2010).
- [17] V.A. Blatov, A.P. Shevchenko, J.V.N. Serezhkin. *Appl. Crystallogr.*, **33**, 1193 (2000).
- [18] A.L. Spek. *Acta Crystallogr., Sect. A*, **46**, 194 (1990).
- [19] K. Biradha, K.V. Domasevitch, B. Moulton, C. Seward, M.J. Zaworotko. *Chem. Commun.*, 1327 (1999); (b) K. Biradha, A. Mondal, B. Moulton, M.J. Zaworotko. *J. Chem. Soc., Dalton Trans.*, 3837 (2000); (c) M.J. Zaworotko. *Chem. Commun.*, 1 (2001); (d) B. Xu, J. Lu, R. Cao. *Cryst. Growth Des.*, **9**, 3003 (2009).
- [20] (a) W. Zhou, X.R. Meng, Y.N. Ding, W.Q. Li, H.W. Hou, Y.L. Song, Y.T. Fan. *J. Mol. Struct.*, **937**, 100 (2009); (b) T.L. Hu, Y. Tao, Z. Chang, X.H. Bu. *Inorg. Chem.*, **50**, 10994 (2011); (c) Z.B. Han, Y.F. Liang, M. Zhou, Y.R. Zhang, L. Li, J. Tong. *CrystEngComm*, **14**, 6952 (2012).
- [21] (a) D. Sun, N. Zhang, R.B. Huang, L.S. Zheng. *Cryst. Growth Des.*, **10**, 3699 (2010); (b) J. Lu, K. Zhao, Q.R. Fang, J.Q. Xu, J.H. Yu, X. Zhang, H.Y. Bie, T.G. Wang. *Cryst. Growth Des.*, **5**, 1091 (2005); (c) X.Q. Yao, M.D. Zhang, J.S. Hu, Y.Z. Li, Z.J. Guo, H.G. Zheng. *Cryst. Growth Des.*, **11**, 3039 (2011).